HDAC3 deacetylates the DNA mismatch repair factor MutSβ to stimulate triplet repeat expansions

Gregory M. Williams[a], Vasileios Paschalis[b], Janice Ortega[c], Frederick W. Muskett[b], James T. Hodgkinson[d], Guo-Min Li[c], John W. R. Schwabe[b], and Robert S. Lahue[a,e,1]

[a]Centre for Chromosome Biology, National University of Ireland Galway, H9W2TY Galway, Ireland; [b]Leicester Institute of Chemical and Molecular Biology, Department of Molecular and Cell Biology, University of Leicester, LE1 7RH Leicester, United Kingdom; [c]Department of Radiation Oncology, University of Texas Southwestern Medical Center, Dallas, TX 75390; [d]Leicester Institute of Chemical and Molecular Biology, School of Chemistry, University of Leicester, LE1 7RH Leicester, United Kingdom; and [e]Galway Neuroscience Centre, National University of Ireland Galway, H9W2TY Galway, Ireland

Trinucleotide repeat (TNR) expansions cause nearly 20 severe human neurological diseases which are currently untreatable. For some of these diseases, ongoing somatic expansions accelerate disease progression and may influence age of onset. This new knowledge emphasizes the importance of understanding the protein factors that drive expansions. Recent genetic evidence indicates that the mismatch repair factor MutSβ (Msh2-Msh3 complex) and the histone deacetylase HDAC3 function in the same pathway to drive triplet repeat expansions. Here we tested the hypothesis that HDAC3 deacetylates MutSβ and thereby activates it to drive expansions. The HDAC3-selective inhibitor RGFP966 was used to examine its biological and biochemical consequences in human tissue culture cells. HDAC3 inhibition efficiently suppresses repeat expansion without impeding canonical mismatch repair activity. Five key lysine residues in Msh3 are direct targets of HDAC3 deacetylation. In cells expressing Msh3 in which these lysine residues are mutated to arginine, the inhibitory effect of RGFP966 on expansions is largely bypassed, consistent with the direct deacetylation hypothesis. RGFP966 treatment does not alter MutSβ subunit abundance or complex formation but does partially control its subcellular localization. Deacetylation sites in Msh3 overlap a nuclear localization signal, and we show that localization of MutSβ is partially dependent on HDAC3 activity. Together, these results indicate that MutSβ is a key target of HDAC3 deacetylation and provide insights into an innovative regulatory mechanism for triplet repeat expansions. The results suggest expansion activity may be druggable and support HDAC3-selective inhibition as an attractive therapy in some triplet repeat expansion diseases.

histone deacetylase 3 | mismatch repair | triplet repeat expansion

Triplet repeats are tandem runs of three nucleotides that occur naturally in the genome. Most triplet repeats are genetically stable and undergo relatively few expansions (gain of repeats) or contractions (loss of repeats). Some triplet repeats are known to expand and cause nearly 20 human genetic diseases, including Huntington's disease (HD) (1), myotonic dystrophy type 1 (DM1) (2–4), and fragile X syndrome (FXS) (5, 6). Expansions can occur both between generations (inherited expansions) and, for some diseases, within tissues of an individual (somatic expansions) (reviewed in refs. 7–10). The medical importance of triplet repeat expansions has generated significant interest in understanding the mechanisms of expansion and in the potential for therapies that might modulate somatic expansions to alter disease pathology (9, 10).

Analysis of expansions in humans and mice revealed several unique features. First, the frequency of expansions can be very high, sometimes approaching 100% (11). Second, expansions can occur both in proliferating tissues (12–16) and in nonproliferating tissues (17–22). This suggests that at least some expansions arise independently of cellular DNA replication (23, 24). Third, disease-causing expansions appear to be limited to the disease gene locus, with no evidence of significant genetic instability elsewhere in the

genome (25, 26). This fact suggests a highly localized mutagenic event that only affects the triplet repeat itself (7–10). These unusual features of triplet repeat expansions point to unique mechanisms of mutagenesis.

The DNA mismatch repair complex MutSβ (Msh2-Msh3 heterodimer) has been identified as a main driver of both inherited and somatic triplet repeat expansions. Gene knockouts in HD, DM1, and FXS mice clearly demonstrate that both *MSH2* and *MSH3* are required for virtually all expansions (20, 21, 27–34). In addition, naturally occurring single nucleotide polymorphisms (SNPs) in mouse *MSH3* also have clear effects on somatic expansions, with lower expansion frequencies correlating with lower Msh3 protein abundance (35). In contrast, the related mismatch repair complex MutSα (Msh2-Msh6 heterodimer) appears to play almost no role in expansions (28, 30–34, 36). Experiments in yeast (37, 38) and human cell culture (39–42) support the primary role of MutSβ in driving expansions. Together, the results from model systems pinpoint MutSβ as a major driving force for expansions.

The focus on MutSβ was recently underscored by genomewide association studies (GWAS) of patients with HD or other CAG•CTG repeat disorders. Disease age of onset and rate of progression are significantly influenced by polymorphisms in *MSH3* (43–46) and other DNA repair genes (47, 48). A polymorphism in *MSH3* is also associated with levels of somatic instability of the

Significance

Triplet repeat expansions cause nearly 20 inherited neurological diseases. The molecular mechanism of expansions is of interest at two levels. First is the basic science of how triplet repeats expand, and the second is the therapeutic opportunity to treat expansion diseases. This study presents evidence that addresses both areas of interest. We show that the histone deacetylase HDAC3 acts directly on the DNA mismatch repair protein MutSβ to stimulate CAG•CTG repeat expansions. This basic science insight into the mechanism also provides an explanation for how HDAC3 inhibition in Huntington's disease mice leads to suppression of triplet repeat expansions and could therefore be considered as a therapy for Huntington's disease and potentially other CAG•CTG repeat expansion diseases.

expanded CTG repeat in DM1 patients (49). The human GWAS findings have triggered substantial interest in therapies that target the ability of MutSβ to promote somatic expansions as a means of slowing or preventing pathology.

Proteins that potentially regulate MutSβ also drive triplet repeat expansions. The role of histone deacetylases (HDACs) in triplet repeat expansion was first identified in yeast and subsequently in human cells (50). siRNA knockdown or chemical inhibition of the human class I enzyme HDAC3 resulted in loss of most expansions. Knockdown of the class IIa HDAC5 or double knockdowns of HDAC3 and HDAC5 also suppressed expansions (39). The genetic epistasis between HDAC3 and HDAC5 is consistent with the known components of the transcriptional corepressor SMRT/NCoR (51), which contains both HDAC3 and HDAC5 (52). Since HDAC3 has the dominant deacetylase activity, it is likely the complex acts by deacetylating one or more protein targets that lead to enhanced triplet repeat expansions. The counteracting histone acetyl transferase (HAT) appears to be CBP/p300, based on the finding that siRNA knockdown of these HATs stimulated expansions (50).

A functional connection between MutSβ and HDAC3/SMRT is highlighted by genetic data indicating that these factors work in the same pathway to promote CAG•CTG repeat expansion (39). This idea is further supported by studies in HD mice, where treatment with the HDAC3-selective inhibitor RGFP966 significantly reduced striatal CAG repeat expansions in the *HTT* gene (53). The evidence from mammalian systems suggests that HDAC3/SMRT deacetylation might activate MutSβ directly, resulting in expansions. However, there have been no data to evaluate this suggestion. In this study, we investigated the hypothesis that the expansion activity of MutSβ is directly controlled through its acetylation state, and that deacetylation by HDAC3/SMRT activates MutSβ to drive expansions. The hypothesis was evaluated by genetic, biochemical, and pharmacological approaches in cultured human cells and with purified components. Expansions in this system require MutSβ (39, 42); they show specificity for expandable repeat sequences over nonexpandable sequence (CAG repeats versus TAG repeats) (54); and there is a $MSH3^{-/-}$ derivative in which variant Msh3 proteins can be expressed without interference from wild-type Msh3 (42).

Materials and Methods

Immunoblot Analysis. Human SVG-A cells were harvested by washing with ice-cold PBS (phosphate-buffered saline) and resuspended in lysis buffer (0.1% wt/vol SDS [sodium dodecyl sulfate], 0.1% vol/vol Triton X-100, 0.1% wt/vol sodium deoxylcholate, 5 mM ethylenediaminetetraacetic acid, 100 mM phenylmethylsulfonyl fluoride) plus mammalian protease inhibitors (Fisher Scientific 12841640) at 1× concentration. Following a 30-min incubation on ice, cells were sonicated and centrifuged at 16,200 × *g* at 4 °C for 40 min. Supernatant protein concentrations were quantified using the detergent compatible protein assay (Bio-Rad Laboratories). Samples containing 50 to 100 μg of total protein were denatured, then resolved on either 10% SDS/polyacrylamide gel electrophoresis gels (Msh2, Msh3, actin, α-tubulin, HDAC3) or precast 4 to 20% gradient gels (Bio-Rad 4565093) (histone H4, acetylated histone H4). Following transfer to nitrocellulose membrane and blocking, membranes were incubated at 4 °C overnight with 1:1,000 dilutions of primary antibodies: Msh3, BD Biosciences 611390 or Abcam 154251; Msh2, Calbiochem NA26; actin, Sigma-Aldrich A2066; histone H4, Abcam AB31830; acetylated histone H4, Millipore, 06-866; and α-tubulin, Abcam AB6161-100. After washing, membranes were incubated for 1 h with 1:10,000 dilutions of secondary antibodies (Li-Cor Biosciences) IRDye 800CW goat α-mouse IgG P/N 925-32210, or IRDye 800CW goat α-rabbit IgG P/N 925-3211 at room temperature. Visualization and quantification was performed using the Odyssey Infrared Imaging system and software (Li-Cor Biosciences).

Shuttle Vector Assay and Measurement of Trinucleotide Repeat (TNR) Expansion Frequencies. The SVG-A shuttle vector assay has been previously described (55). Briefly, a shuttle vector harboring a (CAG)22 repeat upstream of a CAN1 reporter gene is transfected into human SVG-A cells using Lipofectamine 2000

(Invitrogen-Thermo Fisher Scientific) (*SI Appendix*, Fig. S1A). The transfected cells were treated with either the HDAC3-selective inhibitor RGFP966 from BioMarin Pharmaceutics, Inc (56, 57) or DMSO (dimethyl sulfoxide; Sigma-Aldrich) at a final concentration of 1 μM or 10 μM and incubated for 48 h to allow for potential expansion of the repeat tract. Cells were then harvested and the shuttle vector plasmid recovered and digested with the restriction enzyme DpnI (New England Biolabs). The digested shuttle vector DNA is then transformed into *Saccharomyces cerevisiae* where a genetic selection (His+ CanR) identifies those plasmid molecules with an apparent expansion. Colonies from the selective plates are then investigated by colony PCR to visualize, validate, and size the expansions (55).

Subcellular Fractionation and Sucrose Cushion Experiments. Subcellular fractionation steps were adapted from Dignam et al. (58). SVG-A cells were seeded in T175 flasks (Sarstedt) and incubated for 24 h before treatment with RGFP966. After 24 h, treated cells were trypsinized, collected, and washed twice with ice cold 1× PBS. All subsequent steps were carried out at 4 °C. Cells were then washed with 5× cell pellet volume of 1× buffer A (10 mM Hepes pH 7.9, 1.5 mM MgCl2, 10 mM KCl, 0.5 mM dithiothreitol 1× concentration of mammalian protease inhibitors [Fisher Scientific 12841640]) and centrifuged at 450 × *g* for 5 min. Supernatant was discarded and the cell pellets were resuspended in 2× cell pellet volume of buffer A and put on ice for 20 min to swell. After incubation, an equal volume of buffer A + 1.0% Nonidet P-40 (Sigma-Aldrich) was added to the cells and incubated on ice for 5 min. Nuclei were collected by centrifugation at 450 × *g* for 10 min, and the supernatant (cytoplasmic fraction) was saved for protein quantification and immunoblot analysis. Recovered nuclei were washed several times with buffer A and centrifuged at 450 × *g* for 5 min. Washed pellets were then resuspended in 1 mL of buffer A and layered over 10 mL of 30% sucrose cushion (10 mM Pipes pH 7.0, 10 mM KCl, 1.5 mM MgCl2, 30% wt/vol sucrose, 1× concentration of mammalian protease inhibitors) before being centrifuged at 800 × *g* for 10 min. The supernatant was discarded, and the previous step repeated. The remaining nuclei were resuspended in 1 mL of buffer A and spun down at 450 × *g* for 5 min, washed again in 1× PBS, and centrifuged at 450 × *g* for 5 min. The supernatant was discarded and the remaining nuclei (nuclear fraction) were lysed with 50 to 200 μL of radioimmunoprecipitation assay lysis buffer (see *Immunoblot Analysis* above) and subjected to protein quantification and immunoblot analysis.

Creation of Msh3-5KR Cell Line. The Msh3-5KR variant was generated by site-directed mutagenesis (Q5 site-directed mutagenesis kit, New England Biolabs) using the Msh3 expression plasmid p*GWB20* (Msh3-cDNA in pcDNA3.1 Neo+) to create p*GWB21* (Msh3-5KR-cDNA in pcDNA3.1 Neo+). The mutated plasmid was transformed into NEBStable DH5α *Escherichia coli* (New England Biolabs) and positive p*GWB21* candidates were selected for by ampicillin resistance. Mutations were confirmed by Sanger sequencing (Source Bioscience). SVG-A $Msh3^{-/-}$ cells were cotransfected with p*GWB21* Msh3-5KR expression plasmid and a pMSCV hygro resistance plasmid (Clontech Laboratories) using Lipofectamine 2000 (Thermo Fisher). After a 48-h incubation, cells were resuspended in hygromycin-supplemented media (400 ng/mL) and diluted to 200 cells/10 cm2 dish to allow formation of colonies. The 1× expression of Msh3-5KR was determined by immunoblot analysis, compared to wild-type Msh3 expression using two different antibodies, BD Biosciences 611390 and Abcam 154251.

Creation of Msh3-EGFP and SV40 NLS3-EGFP Fusion Plasmids. Msh3[91-130]-EGFP and Msh3-5KR[91-130]-EGFP fusion proteins were created from plasmids p*GWB20* (Msh3-cDNA in pcDNA3.1 Neo+) and p*GWB21* (Msh3-5KR-cDNA in pcDNA3.1 Neo+). Briefly, PCR was used to amplify the *MSH3* or *MSH3-5KR* coding region from codons 91 to 130 using primers Msh3 91 to 130F and Msh3 91 to 130R (*SI Appendix*, Fig. S1B). Following cleavage with XhoI and AgeI, the PCR products were cloned into the corresponding sites of vector pEGFP-N1 (originally from Clontech; a generous gift of Kevin Sullivan, National University of Ireland, Galway, Ireland). The SV40 nuclear localization signal (NLS) was used as a positive control for nuclear localization. We created an SV40-NLS[3x]-EGFP fusion, with three tandem copies of the NLS sequence PKKKRKV, by enzymatic phosphorylation of oligonucleotides SV40 NLS3 F and SV40 NLS3 R, followed by heating and slow cooling to allow annealing. The duplex product was ligated into the XhoI and AgeI sites of vector pEGFP-N1. To create full-length Msh3-EGFP and Msh3-5KR-EGFP constructs, PCR was performed on the full coding region of *MSH3* or *MSH3-5KR* coding region using primers Msh3 Gibson F and Msh3 Gibson R, followed by Gibson assembly in pEGFP-N1. All plasmid clones were confirmed by DNA sequencing.

Generation of GFP-Msh3 Stable Cell Lines. SVG-A cells were transfected with Lipofectamine 2000 (Thermo Fisher) using 500 ng of either full-length GFP-Msh3 or full-length GFP-Msh3-5KR plasmids and incubated for 48 h. Transfected cells were then subjected to limited dilution (one cell per five wells in 96-well dishes) to obtain a monoclonal cell population of GFP-positive candidates. The 96-well plates were incubated for 14 to 21 d to allow single cells to grow into colonies. GFP-positive colonies were then bulked up to 25 mm² flasks where stable integrations could be confirmed by PCR (*SI Appendix*, Fig. S1*B*) GFP-Msh3 protein expression was measured in individual clones by immunoblot analysis using α-Msh3 (BD Biosciences 611390) and α-GFP antibodies.

Immunofluorescence Microscopy. The 1.2×10^5 SVG-A cells were seeded in six-well tissue culture plates (Sarstedt) containing sterile glass coverslips (Fisher) and 2 mL of complete Dulbecco's modified Eagle media and incubated overnight at 37 °C and 5% CO_2. After ~16 h, cells were treated with either DMSO or RGFP966 at a final concentration of 10 μM for 24 h. Cells were briefly washed with warm 1× PBS, then fixed with warm 4% vol/vol paraformaldehyde (Sigma) for 10 min at 37 °C. After fixation, coverslips were washed again with 1× PBS and air dried. A total of 10 μL of SlowFade Gold plus DAPI (Thermo Fisher) was used to mount each coverslip. Z-stack images were acquired using an Olympus Delta Vision microscope at either 100× or 60× magnification with a 0.5-μm limit per image. Images were processed using Fiji ImageJ software.

Mismatch Repair Assay. HeLa cells were grown to 90% confluence in RPMI (Roswell Park Memorial Institute) 1640 media supplemented with 5% fetal bovine serum. RGFP966 (5 μM) was added to cells 12 h before harvesting. Nuclear extracts were prepare as previously described (59). DNA substrates used for the mismatch repair (MMR) assay are circular heteroduplex containing a single G-T or a 2-nucleotide insertion/deletion (2-ID) mismatch and a strand break 5′ to the DNA lesion (60, 61). In vitro MMR assays were performed as described (62). Briefly, a 20-μL reaction containing 30 fmol DNA substrate and 75 μg nuclear extract was incubated for 15 min at 37 °C. DNA was recovered and digested with *NsiI/ClaI* and *XmcI/ClaI* for the G-T and 2-ID substrates, respectively. Reaction products were visualized by ethidium bromide staining. MMR products were quantified using ImageJ.

DNA Hairpin Repair Assay. HeLa cells were again grown to 90% confluence in RPMI 1640 media supplemented with 5% fetal bovine serum, and RGFP966 (5 μM) was added to cells 12 h before harvesting. Nuclear extracts were prepare as previously described (59). DNA substrates containing a loop or hairpin of 5 or 15 extra CAG repeats were prepared as described (63). Hairpin repair assay was performed in a 40-μL reaction containing 42 fmol of DNA substrate and 100 μg of nuclear extract. Reactions were incubated at 37 °C for 30 min. DNA was recovered and digested using *BglI* and *PstI* before loading to a 6% denaturing polyacrylamide gel to resolve the products. Repair products were visualized by Southern hybridization using a ^{32}P-labeled probe specifically annealing to the nick (repair) strand near the *PstI* site (see Fig. 3*C*). Repair activity was quantified using ImageJ. Graph and statistical analysis was obtained by *t* test analysis using GraphPad Prism.

NMR Experiments. Acetylated peptides (*SI Appendix*, Fig. S2) were dissolved in the same buffer as the gel filtration buffer used to purify the SMRT:HDAC3 complex (10 mM Tris·HCl pH 7.5, 50 mM NaCl) at a concentration of 1.0 mg/mL. NMR samples were prepared containing 200 μM of peptide, 122 nM of SMRT(389-480)/HDAC3 complex, and 8 μM of IP$_6$ in 5% vol/vol D$_2$O (600 μL final volume in a 5-mm Wilmad NMR tube). In vitro deacetylation of the peptide substrates was monitored in real time using successive ^{1}H one-dimensional (1D) spectra. We recorded a reference ^{1}H 1D spectrum in the absence of the complex, by performing four dummy scans and 16 actual scans, leading to a total acquisition time of 61.7 s. The SMRT(389-480)/HDAC3 complex was added to initiate the reaction. A series of ^{1}H 1D spectra with the same parameters with the reference spectrum were recorded for 60 min. The time between the addition of the complex and the acquisition of the first ^{1}H 1D spectrum was monitored (68 s to 81 s, depending on the peptide) was noted down for each experiment. The 1D NMR spectra were acquired using a Bruker Avance 600 MHz. The NMR spectra were processed using "TopSpin" (Bruker). The integrals of the peaks of interest were determined using the "Kinetics Method" in the program "Dynamics Center" (Bruker). As the integral of a peak correlates with the concentration of the protons generating the peak, we were able to quantify the percentage of product over the initial substrate using the equation in *SI Appendix*, Fig. S3*A*.

Statistical Analysis. All *P* values and *n* values for repeat instability, Western blot, and immunoprecipitation experiments are specified in *SI Appendix*, Fig.

S1*C* and, where statistical significance was reached, in the relevant figure legend. Statistical tests used for each *P* value are stated for each figure.

Results

HDAC3 Targets Specific Lysine Residues in Msh3 to Stimulate Triplet Repeat Expansions.
If acetylation and deacetylation of MutSβ control its ability to catalyze triplet repeat expansions, then there should be specific lysine residues in MutSβ which are the targets
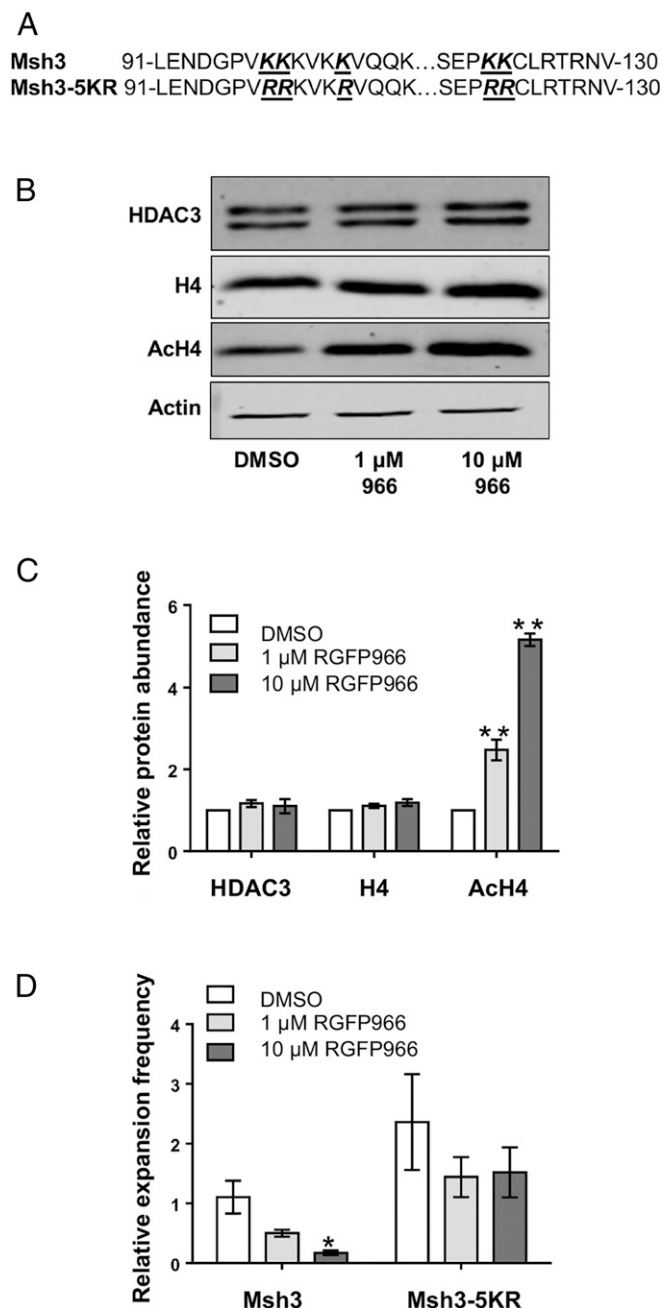

Fig. 1. Putative HDAC3 sites in MutSβ affect triplet repeat expansions. (*A*) Previous proteomic studies (https://www.phosphosite.org//homeAction.action) identified five acetylated lysine residues in Msh3. The Msh3-5KR mutant changes these lysine residues to arginines, mimicking a permanently deacetylated Msh3 protein. (*B*) Representative Western blot after HDAC3 inhibition by RGFP966 treatment. (*C*) Quantification of Western blot signals as a function of RGFP966 dose. **$P < 0.001$, $n = 4$. (*D*) TNR expansions as a function of RGF966 dose in cells expressing Msh3 or Msh3-5KR. *$P < 0.05$, $n = 4$. See *SI Appendix*, Fig. S1*C* for statistical details.

Williams et al.

for this regulation. Information in a proteomics database (https://www.phosphosite.org//homeAction.action) listed acetylated lysine residues, originally identified by proteomics studies (summarized in ref. 64). We focused on the Msh3 subunit since it is specific to MutSβ. Five acetylation sites are clustered in the N terminus of Msh3 (residues K98, K99, K103, K122, and K123) (Fig. 1A). All five lysine residues were mutated to arginine to create the variant protein Msh3-5KR (Fig. 1A) and thereby block acetylation at the five residues. Our hypothesis predicts that Msh3-5KR protein will mimic the deacetylated form of MutSβ and, therefore, cells expressing Msh3-5KR will bypass the requirement for deacetylation by HDAC3. The plasmid with *MSH3-5KR* was stably integrated into the genome of *MSH3−/−* cells (42) and integrants were identified that expressed Msh3-5KR at near wild-type levels (1.1× normal Msh3 level; *SI Appendix*, Fig. S4 *A–D*).

The HDAC3-selective inhibitor RGFP966 was used to block the putative deacetylation of MutSβ. Control experiments showed that the inhibitor was efficacious, with a dose-dependent increase in acetylated histone H4, but with no significant effect on the abundance of either HDAC3 itself or total H4 (Fig. 1 *B* and *C* and *SI Appendix*, Fig. S1C). In triplet repeat expansion assays with cells expressing wild-type Msh3, RGFP966 showed a dose-dependent inhibition of expansions (Fig. 1D and *SI Appendix*, Fig. S1C). Reductions in expansion frequency by approximately 50% and 85% of control values were observed at RGFP966 doses of 1 μM and 10 μM, respectively. The latter expansion value is similar in magnitude to that reported previously when HDAC3 expression was ablated with siRNA (39), supporting the premise that RGFP966 reduces expansions through inhibition of HDAC3. Control experiments indicated that RGFP966 treatment had little effect on cell viability or proliferation (*SI Appendix*, Fig. S5), eliminating the possibility that the inhibitor reduces cell numbers and thereby reduces expansion frequency.

When expansions were tested in cells expressing Msh3-5KR and treated with RGFP966, a different pattern emerged (Fig. 1D). In the absence of inhibitor, the expansion activity was increased compared to cells expressing wild-type Msh3, although the increase was not statistically significant ($P = 0.2215$; *SI Appendix*, Fig. S1C). The increase is consistent with the idea that Msh3-5KR alters the putative acetylation state of MutSβ toward the deacetylated form and therefore causes more expansions. Further differences were observed when RGFP966 was added. While about one-half of the expansions were still sensitive to the inhibitor, the other ~50% of expansions were resistant to HDAC3 inhibition. This effect is most apparent for RGFP966 treatment at 10 μM concentration. The fraction of expansions that are resistant to RGFP966 suggests that the deacetylation-mimic Msh3-5KR obviates the need for HDAC3 and therefore bypasses the effects of the inhibitor. Thus, in the absence of RGFP966, HDAC3 appears to directly deacetylate MutSβ to enhance its expansion activity.

HDAC3 Deacetylates Msh3 Peptides In Vitro. The hypothesis that HDAC3 deacetylates MutSβ predicts that HDAC3 will be active on acetylated peptides from Msh3. Five 15-residue peptides were chemically synthesized with Msh3 protein sequence (Fig. 2A and *SI Appendix*, Fig. S2). Each peptide contained a single acetylated lysine residue in the center. NMR of each peptide gave a peak near 1.83 ppm, characteristic of acetyl-lysine (Fig. 2A). This peak disappeared after treatment with purified SMRT(389-480)/HDAC3 (*SI Appendix*, Fig. S3B) (65), with a subsequent increase in free acetic acid near 1.78 ppm (Fig. 2A). Time course experiments monitored by pseudo two-dimensional (2D) NMR showed that each peptide was deacetylated by HDAC3 but with different apparent rates (Fig. 2B). The K122ac peptide was deacetylated most rapidly, followed by K99ac and K123ac at approximately equal rates, then K98ac and K103ac. The difference in rate between fastest and slowest rates was approximately fourfold. The

relative rates are in general accordance with published data for SMRT/HDAC3 preferences for the two amino acids that follow the acetylated lysine (66). Thus, SMRT(389-480)/HDAC3 is able to bind and deacetylate lysine residues of Msh3 peptides. These results support the model where SMRT/HDAC3 deacetylates key lysine residues in Msh3 to regulate its expansion activity.

Mismatch Repair Activity Is Unaffected by HDAC3 Inhibition. If HDAC3 deacetylates MutSβ to activate it for triplet repeat expansions, is canonical mismatch repair activity also affected? This question was addressed using biochemical assays for mismatch repair. HeLa cells were treated with DMSO as control or 10 μM RGFP966, then nuclear extracts were prepared and analyzed. Immunoblots indicated efficacy of HDAC3 inhibition as histone H3 acetylation was increased at lysine residues 9, 14, and 18 (Fig. 3A). The abundance of mismatch repair proteins Msh2, Msh3, Msh6, Mlh1, and Pms2 appeared unaffected by RGFP966 treatment. When the extracts were assayed for mismatch repair activity, the RGFP966-treated sample showed as much or more mismatch repair on 5′ nicked substrates containing a G-T mismatch or a 2-nt insertion/deletion loop (Fig. 3B). Similarly, alternative substrates with loops of 5 or 15 CAG repeats (Fig. 3C) showed as much or more repair to the loop-retention product in extracts from RGFP966-treated cells (Fig. 3 *D* and *E* and *SI Appendix*, Fig. S1C). By these criteria, HDAC3 inhibition does not interfere with canonical mismatch repair or CAG loop repair.

MutSβ Contains a Potential NLS That Is Sensitive to HDAC3 Activity. Several initial possibilities as to how HDAC3 might regulate MutSβ were tested and rejected. One idea is that HDAC3 regulates transcription of *MSH2* and/or *MSH3*, so inhibition of HDAC3 would alter gene expression and protein abundance. Steady-state levels of Msh2, wild-type Msh3, and Msh3-5KR were examined by immunoblot of extracts prepared from SVG-A cells treated with DMSO alone or increasing doses of RGFP966 (*SI Appendix*, Fig. S4 *A–D*). The results show no significant difference in abundance of Msh2, wild-type Msh3, or Msh3-5KR. This finding is in accord with earlier studies where Msh2 and Msh3 protein levels were unaffected by siRNA knockdown of HDAC3 (39). A second possibility is that HDAC3 regulates MutSβ heterodimer formation or stability. Coimmunoprecipitation (co-IP) experiments showed there was no significant difference in levels of MutSβ complex in extracts of wild-type cells treated with DMSO only or 10 μM RGFP966 (*SI Appendix*, Fig. S4 *E–H*). Co-IP experiments from cells expressing Msh3-5KR showed a slight decrease in MutSβ complex formation, although this difference was not statistically significant (*SI Appendix*, Fig. S4 *E* and *F*). A third mechanism would be if HDAC3 controls access of MutSβ to the triplet repeat DNA; however, previous work using chromatin immunoprecipitation showed that MutSβ occupancy at the TNR was unaltered by siRNA knockdown of HDAC3 (39).

An alternative explanation was suggested by the clustering of the five key lysine residues in Msh3. Perhaps these lysine residues serve as a NLS, and this NLS might be regulated by acetylation. If so, acetylation-dependent partitioning of MutSβ between the nucleus and cytoplasm would provide a mechanism to explain the connection between HDAC3 and triplet repeat expansions. Alignment of a known NLS motif in the Msh6 subunit of MutSα (67, 68) with Msh3 and Msh3-5KR (Fig. 4A) showed that Msh3 lysine residues 98 and 99 align with part of the NLS from Msh6, and that Msh3 lysine 103 also aligns with a cognate lysine in Msh6. The putative NLS in Msh3 overlaps with a strong functional NLS between residues 98 and 107 of Msh3 that was recently described (69). We sought to build on this knowledge with experiments to test the possibility that the acetylation status of lysine residues in the predicted Msh3 NLS controls the subcellular localization of Msh3 and thereby helps regulate triplet repeat expansions.
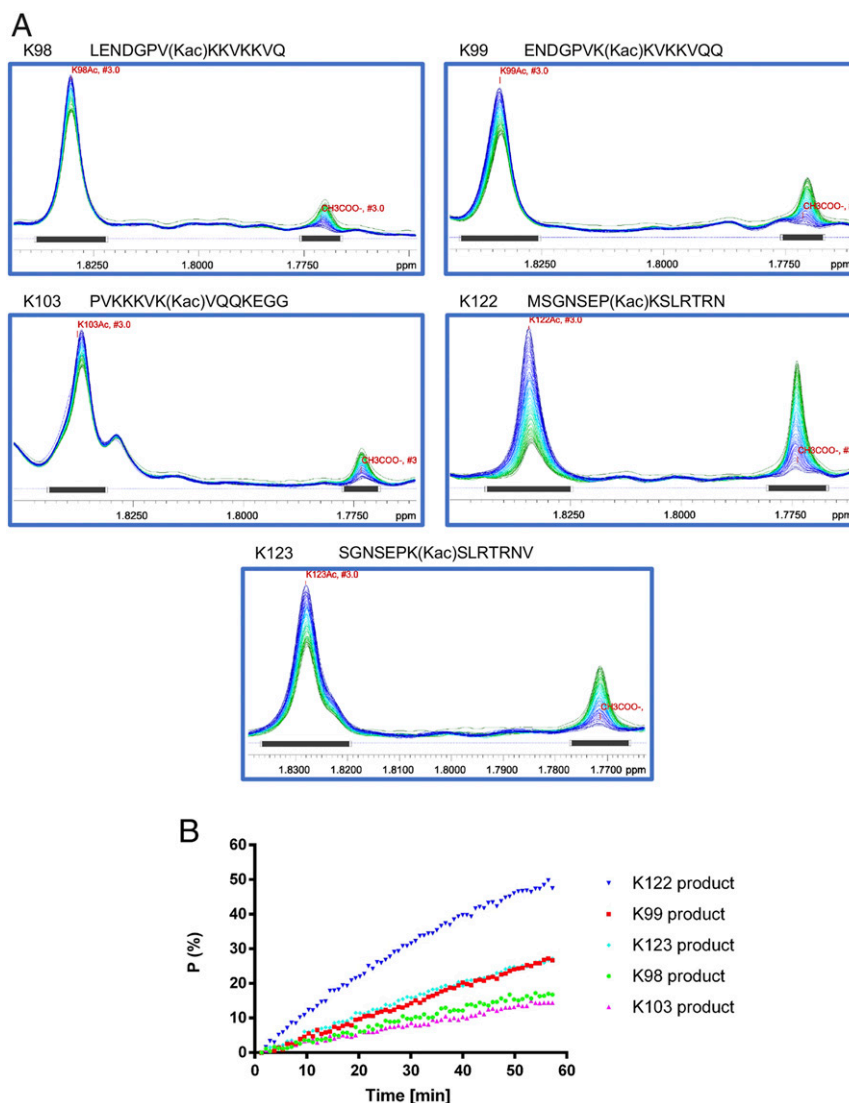
Fig. 2. Deacetylation assays of acetylated peptides derived from Msh3 in the presence of SMRT(389-480)/HDAC3 complex. (*A*) KAc and CH$_3$COO$^-$ peak integral quantification. Dynamics Center (Bruker) interface showing the alignment of peaks corresponding to the acetyl group of the acetylated lysines (substrate, ~1.83 ppm) and the free acetic acid (product, ~1.78 ppm) after incubation with SMRT(389-480)/HDAC3 at 20 °C for 60 min. (*B*) SMRT(389-480)/ HDAC3 complex preferentially deacetylates Msh3 K122 peptide over the rest of the substrates. The ratio of the integrals of the products (free acetic acid) over the integrals of the substrates (acetyl group of lysines) was plotted against reaction time.

Subcellular fractionation experiments tested whether MutSβ relocates, in whole or in part, from nucleus to cytoplasm when HDAC3 is inhibited. In cells expressing wild-type Msh3, both Msh3 and Msh2 were predominantly located in the nucleus without any HDAC3 inhibitor (Fig. 4 *B* and *D* and *SI Appendix,* Fig. S1*C*). Only 2% and 15% of Msh3 and Msh2, respectively, fractionated with the cytoplasm. However, treatment of the cells with RGFP966 caused an additional 10% of both subunits to shift to the cytoplasm (Fig. 4 *B* and *D* and *SI Appendix,* Fig. S1*C*). In contrast, cells expressing Msh3-5KR showed no detectable difference in cytoplasmic localization with or without RGFP966 (Fig. 4 *C* and *E*). These data offer an explanation for the ability of cells with Msh3-5KR to partially resist the effects of HDAC3 inhibition by partly blocking the relocalization of MutSβ to the cytoplasm. Immunofluorescence (IF) microscopy provided additional support. We constructed fusions of Msh3 amino acid residues 91 to 130, the region containing the five lysine residues of interest, with EGFP. Transient transfection showed that an EGFP-only control was distributed throughout the cell, while fusion of the SV40 large T antigen NLS to EGFP resulted in nuclear localization (Fig. 5*A*). Neither control fusion protein showed substantial alteration in localization upon treatment with RGFP966. Fusion of wild-type Msh3[91-130] to EGFP resulted in primarily nuclear localization, but a significant amount of fluorescence was shifted to the cytoplasm upon the addition of RGFP966. In contrast, Msh3-5KR[91-130]-EGFP remained predominantly nuclear even when the HDAC3 inhibitor was added (Fig. 5*A*). IF experiments were also performed on cells with stably integrated, full-length fusions of wild-type Msh3-EGFP or Msh3-5KR-EGFP. Wild-type Msh3-EGFP was predominantly nuclear with DMSO addition but some fluorescence was observed in the cytoplasm with RGFP966 treatment (Fig. 5*B*). The extent of the relocalization appeared to be in line with the subcellular localization experiments (Fig. 4). In contrast, the IF images with full-length Msh3-5KR-EGFP showed no apparent relocalization of nuclear fluorescence intensity with RGFP966 treatment (Fig. 5*C*). In total, the subcellular fractionation and IF images support a model where at least some MutSβ relocalizes from the nucleus to the cytoplasm with HDAC3 inhibition.
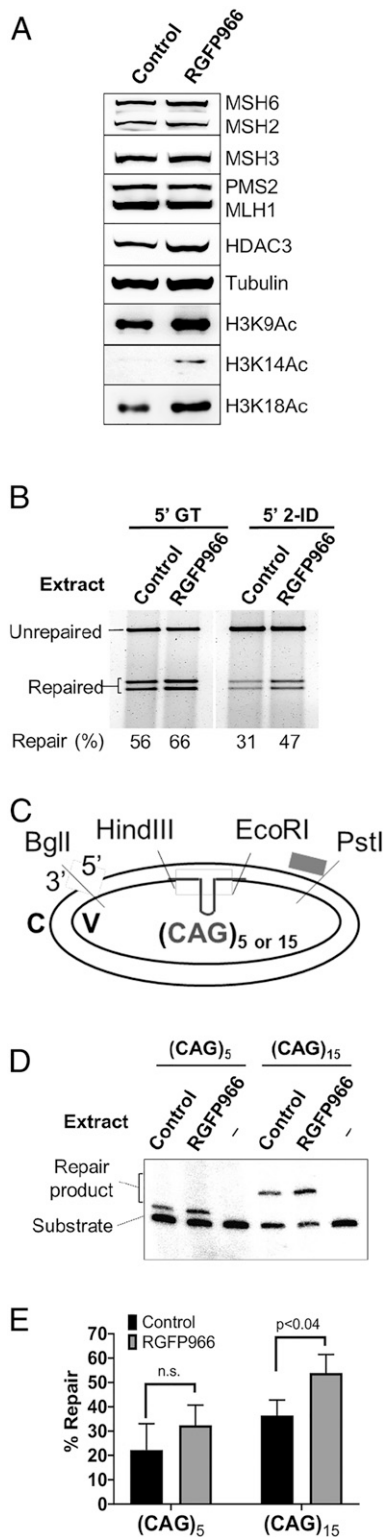
Williams et al.

www.manaraa.com

Fig. 3. DNA mismatch repair and DNA hairpin repair assays after RGFP966 treatment. (*A*) Western blots showing expression of MMR proteins and related histone marks. (*B*) In vitro MMR assay using a 5′ nicked heteroduplex containing a G-T mismatch or a 2-nt insertion/deletion mispair. The % of repair represents the average repair of three independent experiments. (*C*) Diagram of DNA substrate containing a (CAG)$_5$ or (CAG)$_{15}$ hairpin structure in the continuous strand. (*D*) Southern blot analysis showing nick-directed hairpin repair. (*E*) Quantification of hairpin repair. $P < 0.04$, $n = 3$. n.s., not significant. See *SI Appendix*, Fig. S1C for statistical details.

This redistribution is mostly blocked by replacement of the five key lysine residues with arginines.

Discussion

This study reveals the biological consequence of HDAC3 activation of MutSβ in triplet repeat expansions and suggests a molecular mechanism connecting HDAC3 to DNA mutagenesis at disease-causing genes. Using the selective inhibitor RGFP966, we demonstrated that HDAC3 inhibition prevents triplet repeat expansion in human cells without hindering canonical mismatch repair activity. Importantly, expansions in cells with five lysine-to-arginine mutations in the Msh3 protein (Msh3-5KR) were largely insensitive to HDAC3 inhibition, consistent with the idea that some or all of the five lysine residues in Msh3 are key targets of HDAC3 deacetylation. The loss of some expansions in the presence of RGFP966 is presumably due to other sites of HDAC3 action, possibly additional residues in Msh3, Msh2, or in other proteins. We also show that purified SMRT(389-480)/HDAC3 complex deacetylates Msh3 peptide substrates containing the five lysines. One outcome of HDAC3 action is to partially control the nuclear localization of MutSβ. Immunofluorescence microscopy and subcellular localization approaches revealed that the deacetylation sites in Msh3 overlap a nuclear localization signal (69). Cells expressing wild-type Msh3 sequences showed nuclear localization that was reduced, although not eliminated, by addition of RGFP966. In contrast, expression of Msh3-5KR led to retention of protein nuclear localization even after treatment with the HDAC3 inhibitor. Together, our findings suggest an innovative regulatory mechanism for TNR expansion involving direct deacetylation of MutSβ by HDAC3. This work underscores HDAC3-selective inhibition as a potential therapy in Huntington's disease and some related CAG•CTG expansion diseases.

This study reports regulation of MutSβ by HDACs, specifically the class I enzyme HDAC3, assisted by the class IIa protein HDAC5 (39). In contrast, the Msh2-Msh6 complex MutSα is regulated by the class IIb enzyme HDAC6 through effects on Msh2 protein stability (70). A different class IIb enzyme, HDAC10, also interacts with Msh2, and MutSα-dependent MMR activity correlates positively with HDAC10 expression levels (71). The MutL homolog Mlh1 undergoes deacetylation by HDAC6 (72), which leads to blockage of assembly of MutSα-MutLα. In summary, there is precedent for class IIb HDAC-dependent regulation of MutSα and MutLα in canonical mismatch repair and response to DNA damage. Our work indicates that MutSβ is activated by class I HDAC3 and class IIa HDAC5 (39), leading to enhanced triplet repeat expansions. We note that the expansion outcome as a function of RGFP966 concentration appears to be dose dependent for Msh3 but less so for Msh3-5KR (Fig. 1*D*). This could be a technical limitation in measuring expansion frequencies. Alternatively, it could be that deacetylation of other lysine sites outside of Msh3 is readily inhibited with RGFP966 at 1 μM concentration, thus blocking approximately one-half of expansions equally well for both Msh3 and Msh3-5KR. In contrast, 10 μM RGFP966 is required to inhibit deacetylation of the five key sites in Msh3 to block the other approximate half of expansions. The Msh3-5KR substitutions would prevent the effect of higher inhibitor dose. The flattening of the response curve for Msh3-5KR could be explained by this possibility.

The fact that MutSβ abundance and complex formation are not altered by HDAC3 inhibition suggests an innovative regulatory mechanism for TNR expansion involving, in part, HDAC3-mediated nuclear localization of MutSβ. This hypothesis is largely consistent with studies on localization of MutSα (68, 73, 74). Mouse and human Msh2 do not contain a putative NLS (73, 74), suggesting that MutSα nuclear import is completely dependent on the Msh6 subunit. Msh6 contains three NLSs that allow for MutSα import into the nucleus (68). The Msh6 NLSs are clustered in the N-terminal
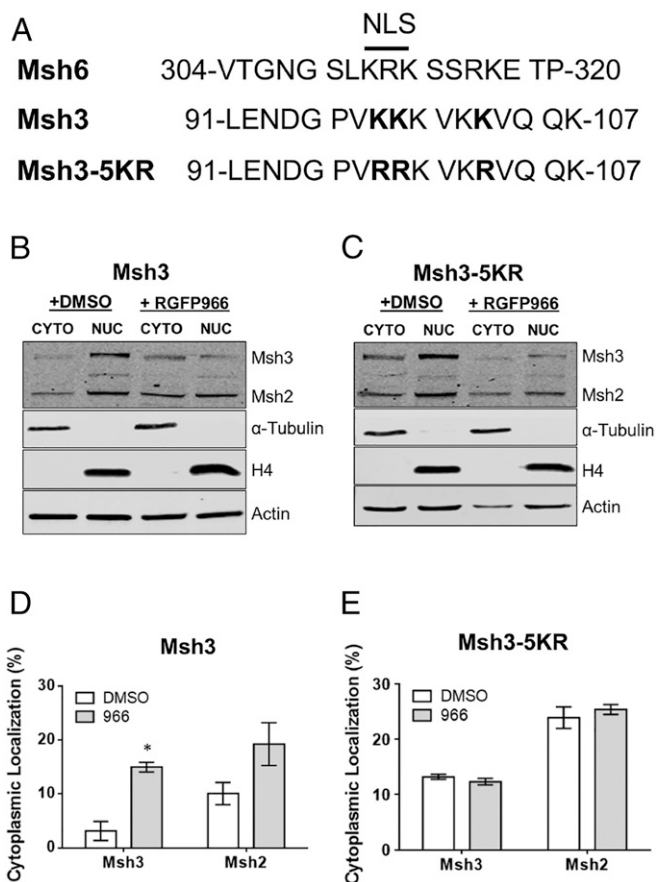
Fig. 4. Subcellular fractionation of MutSβ following treatment with RGFP966. (*A*) Sequence alignment of a known NLS in Msh6 (67, 68) with Msh3 and Msh3-5KR. Msh3 residues 98, 99, and 103 are shown in boldface. (*B*) Representative Western blot of subcellular fractionation of MutSβ. (*C*) Representative Western blot of subcellular fractionation of MutSβ containing Msh3-5KR. (*D*) Quantification of subcellular fractionation experiments performed in Msh3-expressing cells. Graph depicts percentage of total Msh3 or Msh2 protein that is localized to the cytoplasm. *$P = 0.0183$, $n = 3$, *SI Appendix*, Fig. S1C. (*E*) Quantification of subcellular fractionation experiments performed in Msh3-5KR-expressing cells. Graph depicts percentage of total Msh3 or Msh2 protein that is localized to the cytoplasm, $n = 3$.

region of the protein and share some sequence homology with the N terminus of Msh3. It was this homology that guided our thinking with respect to potential NLS activity in Msh3 (Fig. 4*A*). Another group recently reported NLS activity in this same Msh3 motif (69). They showed that the strongest NLS in Msh3 is between residues 84 and 107, with particular requirement for the region 98 to 107. Our results are in agreement with this conclusion (*SI Appendix*, Fig. S6). We go on to show that NLS activity in MutSβ is regulated in part by HDAC3 deacetylation of five lysine residues between residues 98 and 123. One challenge in interpreting this information is that the N-terminal 220 amino acids of Msh appear to be largely unstructured, based on bioinformatics analysis (*SI Appendix*, Fig. S3 *C* and *D*). As HDAC3 inhibition suppresses most expansions but its effect on MutSβ localization is only partial, we speculate there could be a subpopulation of MutSβ that is responsible for triplet repeat expansions that is also sensitive to cellular relocalization in response to changes in its acetylation status.

A model is presented to suggest how acetylation/deacetylation of MutSβ affects triplet repeat expansions (Fig. 6). Import of MutSβ into the nucleus via the lysine-rich Msh3 NLS allows acetylation by p300/CBP and deacetylation by SMRT/HDAC3. In this model, deacetylated MutSβ can shuttle freely between the

cytoplasm and the nucleus, allowing nuclear MutSβ access to triplet repeat DNA to drive expansions. This condition predominates in the presence of the Msh3-5KR mutant that mimics the deacetylated state. In contrast, acetylated MutSβ can exit the nucleus but its reentry is inhibited. This reduces the level of nuclear MutSβ, limits its access to triplet repeat DNA, and helps suppress expansions. This condition is simulated when cells are treated with RGFP966. There is precedent for the idea that protein acetylation regulates nuclear localization. NLS acetylation has been identified as a molecular toggle for the IFN-inducible viral DNA sensor IFI16, inhibiting its nuclear import (75). Acetylation of a lysine in the NLS of c-Abl drives cytoplasmic accumulation (76). For other proteins, lysine acetylation is required for nuclear localization and retention, including the eukaryotic translation initiation factor 5A (77) and retinoblastoma protein (78). The impact of acetylation on NLS function seems versatile, either promoting or preventing nuclear import.

Another possibility for HDAC3/SMRT control of expansions is that the acetylation status of MutSβ affects its binding to triplet repeat hairpins or other alternative secondary structures that are thought to be intermediates in expansions (7–10). This explanation would help tie acetylation of MutSβ to structure-forming triplet repeats, which coincide with the subset of sequences known to
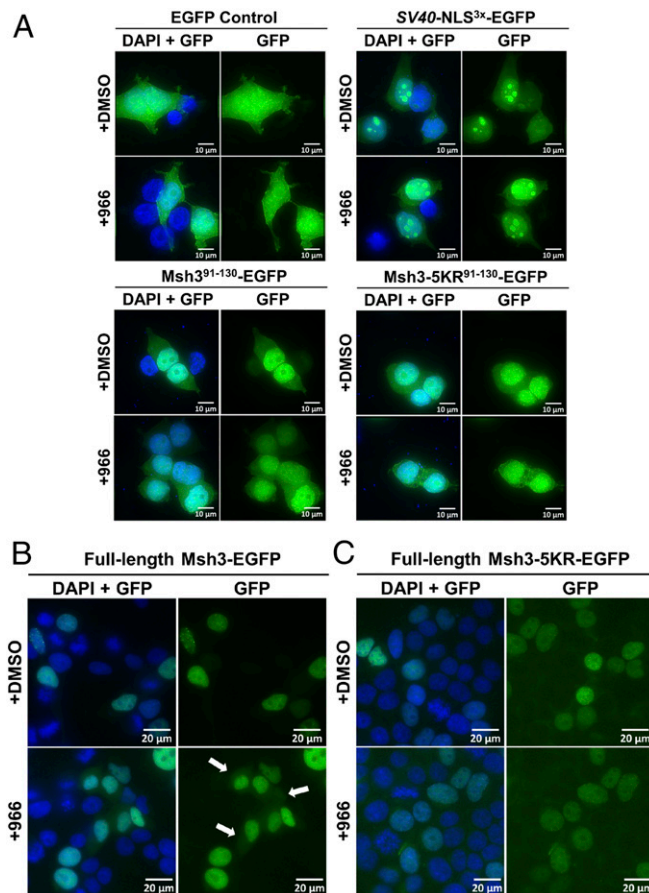
Fig. 5. Immunofluorescence microscopy using EGFP tags. In all panels, DAPI + GFP indicates overlay of separate imaging for DAPI and EGFP. When present, RGFP966 dose was 10 μM. Scale bars are indicated in each image. (*A*) Transient transfections of EGFP fusion peptides. *Top Left*, EGFP alone; *Top Right*, SV40-NLS³ˣ-EGFP positive control; *Bottom Left*, Msh3⁹¹⁻¹³⁰-EGFP; *Bottom Right*, Msh3-5KR⁹¹⁻¹³⁰-EGFP. FITC channel for EGFP signal. (*B*) Stable transfectants expressing full-length Msh3-EGFP. White arrows indicate cytoplasmic accumulation of fluorescent protein. (*C*) Stable transfectants expressing full-length Msh3-5KR-EGFP.
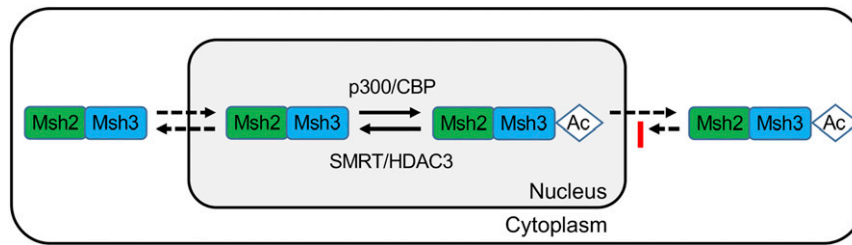
Williams et al.

www.manaraa.com

Fig. 6. Model for SMRT/HDAC3 control of MutSβ subcellular localization. MutSβ is able to translocate into the nucleus due to the nuclear localization sequence in Msh3. Inside the nucleus, MutSβ is subject to acetylation by p300/CBP and deacetylation by SMRT/HDAC3. The deacetylated form of MutSβ can translocate in and out of the nucleus (*Left*). MutSβ containing Msh3-5KR simulates this situation. In contrast, the acetylated form of MutSβ can exit the nucleus (*Right*) but its reentry occurs with reduced efficiency (red vertical bar). Treatment with RGFP966 favors acetylated MutSβ, hinders its nuclear reentry, and thereby suppresses triplet repeat expansions.

expand and cause disease (79). Alternatively, protein-protein interactions between MutSβ and other proteins involved in expansions might be subject to modulation by acetylation-deacetylation. Developing suitable assays for these activities presents an interesting challenge going forward.

While triplet repeat expansions were very sensitive to RGFP966 inhibition of HDAC3, canonical mismatch repair and CAG loop repair activities were slightly stimulated by the inhibitor. The most likely explanation is that MutSα, the predominant complex in HeLa cells (80), is not affected by HDAC3 inhibition and thereby masks any effects on the lower-abundance MutSβ in these repair assays. This interpretation is consistent with the known dependence of G-T repair on MutSα and the overlap in repair activity between MutSα and MutSβ for 2-nt looped substrates (80, 81). CAG loop repair does not require MutSβ (63, 82). Nonetheless, the retention of canonical repair activity after HDAC3 inhibition suggests there may be no genetic price to pay in therapeutic approaches to expansions using RGFP966.

Our findings are also relevant to recent GWAS findings that genetic variation in *MSH3* influences somatic expansions and disease severity in HD and DM1 (43–46). Increased *MSH3* expression is associated with disease progression in both diseases (44, 46), helping support the conclusion that the timing of

disease onset is determined, in part, by Msh3-dependent expansions of CAG•CTG repeats (46). Additional support came from a study in HD mice that traced strain-dependent differences in CAG somatic repeat instability to polymorphisms in *MSH3* primarily affecting Msh3 protein stability (35). Direct activation of MutSβ by HDAC3 also provides a mechanistic explanation for how RGFP966 treatment of HD mice suppressed striatal instability in the *HTT* CAG repeat (53). It is a reasonable inference that RGFP966 inhibition of HDAC3 in vivo prevented deacetylation of Msh3 and thereby blocked MutSβ in driving repeat expansion. Therefore, a direct mechanistic connection is feasible between HDAC3 inhibition and slowing somatic repeat expansion to alter the course of triplet repeat expansion disease.

Data Availability. All study data are included in the article and *SI Appendix*.

1. The Huntington's Disease Collaborative Research Group, A novel gene containing a trinucleotide repeat that is expanded and unstable on Huntington's disease chromosomes. *Cell* **72**, 971–983 (1993).
2. J. D. Brook *et al.*, Molecular basis of myotonic dystrophy: Expansion of a trinucleotide (CTG) repeat at the 3′ end of a transcript encoding a protein kinase family member. *Cell* **68**, 799–808 (1992).
3. Y.-H. Fu *et al.*, An unstable triplet repeat in a gene related to myotonic muscular dystrophy. *Science* **255**, 1256–1258 (1992).
4. M. Mahadevan *et al.*, Myotonic dystrophy mutation: An unstable CTG repeat in the 3′ untranslated region of the gene. *Science* **255**, 1253–1255 (1992).
5. E. J. Kremer *et al.*, Mapping of DNA instability at the fragile X to a trinucleotide repeat sequence p(CCG)n. *Science* **252**, 1711–1714 (1991).
6. A. J. Verkerk *et al.*, Identification of a gene (FMR-1) containing a CGG repeat coincident with a breakpoint cluster region exhibiting length variation in fragile X syndrome. *Cell* **65**, 905–914 (1991).
7. K. Usdin, N. C. House, C. H. Freudenreich, Repeat instability during DNA repair: Insights from model systems. *Crit. Rev. Biochem. Mol. Biol.* **50**, 142–167 (2015).
8. R. R. Iyer, A. Pluciennik, M. Napierala, R. D. Wells, DNA triplet repeat expansion and mismatch repair. *Annu. Rev. Biochem.* **84**, 199–226 (2015).
9. M. H. M. Schmidt, C. E. Pearson, Disease-associated repeat instability and mismatch repair. *DNA Repair (Amst.)* **38**, 117–126 (2016).
10. A. N. Khristich, S. M. Mirkin, On the wrong DNA track: Molecular mechanisms of repeat-mediated genome instability. *J. Biol. Chem.* **295**, 4134–4170 (2020).
11. E. P. Leeflang *et al.*, Analysis of germline mutation spectra at the Huntington's disease locus supports a mitotic mutation mechanism. *Hum. Mol. Genet.* **8**, 173–183 (1999).
12. L. Zhang, E. P. Leeflang, J. Yu, N. Arnheim, Studying human mutations by sperm typing: Instability of CAG trinucleotide repeats in the human androgen receptor gene. *Nat. Genet.* **7**, 531–535 (1994).
13. E. P. Leeflang *et al.*, Single sperm analysis of the trinucleotide repeats in the Huntington's disease gene: Quantification of the mutation frequency spectrum. *Hum. Mol. Genet.* **4**, 1519–1526 (1995).
14. M. Zatz *et al.*, Analysis of the CTG repeat in skeletal muscle of young and adult myotonic dystrophy patients: When does the expansion occur? *Hum. Mol. Genet.* **4**, 401–406 (1995).
15. L. Martorell *et al.*, Germline mutational dynamics in myotonic dystrophy type 1 males: Allele length and age effects. *Neurology* **62**, 269–274 (2004).
16. C. Savouret *et al.*, MSH2-dependent germinal CTG repeat expansions are produced continuously in spermatogonia from DM1 transgenic mice. *Mol. Cell. Biol.* **24**, 629–637 (2004).
17. H. Telenius *et al.*, Somatic and gonadal mosaicism of the Huntington disease gene CAG repeat in brain and sperm. *Nat. Genet.* **6**, 409–414 (1994).
18. C. A. Thornton, K. Johnson, R. T. Moxley 3rd, Myotonic dystrophy patients have larger CTG expansions in skeletal muscle than in leukocytes. *Ann. Neurol.* **35**, 104–107 (1994).
19. M. T. Fortune, C. Vassilopoulos, M. I. Coolbaugh, M. J. Siciliano, D. G. Monckton, Dramatic, expansion-biased, age-dependent, tissue-specific somatic mosaicism in a transgenic mouse model of triplet repeat instability. *Hum. Mol. Genet.* **9**, 439–445 (2000).
20. I. V. Kovtun, C. T. McMurray, Trinucleotide expansion in haploid germ cells by gap repair. *Nat. Genet.* **27**, 407–411 (2001).
21. C. Savouret *et al.*, CTG repeat instability and size variation timing in DNA repair-deficient mice. *EMBO J.* **22**, 2264–2273 (2003).
22. R. Gonitel *et al.*, DNA instability in postmitotic neurons. *Proc. Natl. Acad. Sci. U.S.A.* **105**, 3467–3472 (2008).
23. M. Gomes-Pereira, M. T. Fortune, D. G. Monckton, Mouse tissue culture models of unstable triplet repeats: *In vitro* selection for larger alleles, mutational expansion bias and tissue specificity, but no association with cell division rates. *Hum. Mol. Genet.* **10**, 845–854 (2001).
24. M. Gomes-Pereira *et al.*, Disease-associated CAG·CTG triplet repeats expand rapidly in non-dividing mouse cells, but cell cycle arrest is insufficient to drive expansion. *Nucleic Acids Res.* **42**, 7047–7056 (2014).
25. M.-Y. Chung *et al.*, Evidence for a mechanism predisposing to intergenerational CAG repeat instability in spinocerebellar ataxia type I. *Nat. Genet.* **5**, 254–258 (1993).

Williams et al.

www.manaraa.com

26. G. M. Goellner et al., Different mechanisms underlie DNA instability in Huntington disease and colorectal cancer. *Am. J. Hum. Genet.* **60**, 879–890 (1997).

27. K. Manley, T. L. Shirley, L. Flaherty, A. Messer, Msh2 deficiency prevents *in vivo* somatic instability of the CAG repeat in Huntington disease transgenic mice. *Nat. Genet.* **23**, 471–473 (1999).

28. W. J. A. A. van den Broek et al., Somatic expansion behaviour of the (CTG)n repeat in myotonic dystrophy knock-in mice is differentially affected by Msh3 and Msh6 mismatch-repair proteins. *Hum. Mol. Genet.* **11**, 191–198 (2002).

29. V. C. Wheeler et al., Mismatch repair gene Msh2 modifies the timing of early disease in Hdh(Q111) striatum. *Hum. Mol. Genet.* **12**, 273–281 (2003).

30. B. A. L. Owen et al., (CAG)(n)-hairpin DNA binds to Msh2-Msh3 and changes properties of mismatch recognition. *Nat. Struct. Mol. Biol.* **12**, 663–670 (2005).

31. L. Foiry et al., Msh3 is a limiting factor in the formation of intergenerational CTG expansions in DM1 transgenic mice. *Hum. Genet.* **119**, 520–526 (2006).

32. E. Dragileva et al., Intergenerational and striatal CAG repeat instability in Huntington's disease knock-in mice involve different DNA repair genes. *Neurobiol. Dis.* **33**, 37–47 (2009).

33. R. A. Lokanga, X. N. Zhao, K. Usdin, The mismatch repair protein MSH2 is rate limiting for repeat expansion in a fragile X premutation mouse model. *Hum. Mutat.* **35**, 129–136 (2014).

34. X.-N. Zhao et al., Muts β generates both expansions and contractions in a mouse model of the Fragile X-associated disorders. *Hum. Mol. Genet.* **24**, 7087–7096 (2015).

35. S. Tomé et al., MSH3 polymorphisms and protein levels affect CAG repeat instability in Huntington's disease mice. *PLoS Genet.* **9**, e1003280 (2013).

36. X. N. Zhao et al., A MutSβ-dependent contribution of MutSβ to repeat expansions in fragile X premutation mice? *PLoS Genet.* **12**, e1006190 (2016).

37. A. Kantartzis et al., Msh2-Msh3 interferes with Okazaki fragment processing to promote trinucleotide repeat expansions. *Cell Rep.* **2**, 216–222 (2012).

38. G. M. Williams, J. A. Surtees, MSH3 promotes dynamic behavior of trinucleotide repeat tracts in vivo. *Genetics* **200**, 737–754 (2015).

39. A.-M. M. Gannon, A. Frizzell, E. Healy, R. S. Lahue, MutSβ and histone deacetylase complexes promote expansions of trinucleotide repeats in human cells. *Nucleic Acids Res.* **40**, 10324–10333 (2012).

40. J. Du, E. Campau, C. Soragni, C. Jespersen, J. M. Gottesfeld, Length-dependent CTG·CAG triplet-repeat expansion in myotonic dystrophy patient-derived induced pluripotent stem cells. *Hum. Mol. Genet.* **22**, 5276–5287 (2013).

41. R. Nakatani, M. Nakamori, H. Fujimura, H. Mochizuki, M. P. Takahashi, Large expansion of CTG•CAG repeats is exacerbated by MutSβ in human cells. *Sci. Rep.* **5**, 11020 (2015).

42. N. Keogh, K. Y. Chan, G. M. Li, R. S. Lahue, MutSβ abundance and Msh3 ATP hydrolysis activity are important drivers of CTG•CAG repeat expansions. *Nucleic Acids Res.* **45**, 10068–10078 (2017).

43. D. J. H. Moss et al.; TRACK-HD investigators; REGISTRY investigators, Identification of genetic variants associated with Huntington's disease progression: A genome-wide association study. *Lancet Neurol.* **16**, 701–711 (2017).

44. M. Flower et al., MSH3 modifies somatic instability and disease severity in Huntington's and myotonic dystrophy type 1. *Brain* **142**, 1876–1886 (2020).

45. M. Ciosi et al.; TRACK-HD team; Enroll-HD team, A genetic association study of glutamine-encoding DNA sequence structures, somatic CAG expansion, and DNA repair gene variants, with Huntington disease clinical outcomes. *EBioMedicine* **48**, 568–580 (2019).

46. Genetic Modifiers of Huntington's Disease (GeM-HD) Consortium, CAG repeat not polyglutamine length determines timing of Huntington's disease onset. *Cell* **178**, 887–900.e14 (2019).

47. Genetic Modifiers of Huntington's Disease (GeM-HD) Consortium, Identification of genetic factors that modify clinical onset of Huntington's disease. *Cell* **162**, 516–526 (2015).

48. L. Jones, H. Houlden, S. J. Tabrizi, DNA repair in the trinucleotide repeat disorders. *Lancet Neurol.* **16**, 88–96 (2017).

49. F. Morales et al., A polymorphism in the MSH3 mismatch repair gene is associated with the levels of somatic instability of the expanded CTG repeat in the blood DNA of myotonic dystrophy type 1 patients. *DNA Repair (Amst.)* **40**, 57–66 (2016).

50. K. Debacker et al., Histone deacetylase complexes promote trinucleotide repeat expansions. *PLoS Biol.* **10**, e1001257 (2012).

51. J. Oberoi et al., Structural basis for the assembly of the SMRT/NCoR core transcriptional repression machinery. *Nat. Struct. Mol. Biol.* **18**, 177–184 (2011).

52. G. M. Hudson, P. J. Watson, L. Fairall, A. G. Jamieson, J. W. Schwabe, Insights into the recruitment of Class IIa histone deacetylases (HDACs) to the SMRT/NCoR transcriptional repression complex. *J. Biol. Chem.* **290**, 18237–18244 (2015).

53. N. Suelves et al., An HDAC3-selective inhibitor delivers concurrent benefits in Huntington's disease mice by preventing cognitive decline and suppressing somatic CAG repeat expansions. *Sci. Rep.* **7**, 6082 (2017).

54. D. A. Claassen, R. S. Lahue, Expansions of CAG.CTG repeats in immortalized human astrocytes. *Hum. Mol. Genet.* **16**, 3088–3096 (2007).

55. G. M. Williams, R. S. Lahue, Assessing triplet repeat expansions in human SVG-A cell culture. *Methods Mol. Biol.* **2056**, 151–172 (2020).

56. M. Malvaez et al., HDAC3-selective inhibitor enhances extinction of cocaine-seeking behavior in a persistent manner. *Proc. Natl. Acad. Sci. U.S.A.* **110**, 2647–2652 (2013).

57. H. Jia et al., The effects of pharmacological inhibition of histone deacetylase 3 (HDAC3) in Huntington's disease mice. *PLoS One* **11**, e0152498 (2016).

58. J. D. Dignam et al., Accurate transcription initiation by RNA polymerase II in a soluble extract from isolated mammalian nuclei. *Nucleic Acids Res.* **11**, 1475–1489 (1983).

59. J. Holmes Jr., S. Clark, P. Modrich, Strand-specific mismatch correction in nuclear extracts of human and *Drosophila melanogaster* cell lines. *Proc. Natl. Acad. Sci. U.S.A.* **87**, 5837–5841 (1990).

60. S. Guo et al., Differential requirement for proliferating cell nuclear antigen in 5′ and 3′ nick-directed excision in human mismatch repair. *J. Biol. Chem.* **279**, 16912–16917 (2004).

61. R. Parsons et al., Hypermutability and mismatch repair deficiency in RER⁺ tumor cells. *Cell* **75**, 1227–1236 (1993).

62. J. Ortega et al., Phosphorylation of PCNA by EGFR inhibits mismatch repair and promotes misincorporation during DNA synthesis. *Proc. Natl. Acad. Sci. U.S.A.* **112**, 5667–5672 (2015).

63. T. Zhang, J. Huang, L. Gu, G. M. Li, In vitro repair of DNA hairpins containing various numbers of CAG/CTG trinucleotide repeats. *DNA Repair (Amst.)* **11**, 201–209 (2012).

64. P. V. Hornbeck et al., PhosphoSitePlus, 2014: Mutations, PTMs and recalibrations. *Nucleic Acids Res.* **43**, D512–D520 (2015).

65. P. J. Watson, L. Fairall, G. M. Santos, J. W. Schwabe, Structure of HDAC3 bound to co-repressor and inositol tetraphosphate. *Nature* **481**, 335–340 (2012).

66. Z. A. Gurard-Levin, K. A. Kilian, J. Kim, K. Bähr, M. Mrksich, Peptide arrays identify isoform-selective substrates for profiling endogenous lysine deacetylase activity. *ACS Chem. Biol.* **5**, 863–873 (2010).

67. M. Christmann, B. Kaina, Nuclear translocation of mismatch repair proteins MSH2 and MSH6 as a response of cells to alkylating agents. *J. Biol. Chem.* **275**, 36256–36262 (2000).

68. N. R. Gassman et al., Cooperative nuclear localization sequences lend a novel role to the N-terminal region of MSH6. *PLoS One* **6**, e17907 (2011).

69. S. S. Tseng-Rogenski et al., The human DNA mismatch repair protein MSH3 contains nuclear localization and export signals that enable nuclear-cytosolic shuttling in response to inflammation. *Mol. Cell. Biol.* **40**, e00029-20 (2020).

70. M. Zhang et al., HDAC6 deacetylates and ubiquitinates MSH2 to maintain proper levels of MutSα. *Mol. Cell* **55**, 31–46 (2014).

71. R. Radhakrishnan et al., Histone deacetylase 10 regulates DNA mismatch repair and may involve the deacetylation of MutS homolog 2. *J. Biol. Chem.* **290**, 22795–22804 (2015).

72. M. Zhang et al., HDAC6 regulates DNA damage response via deacetylating MLH1. *J. Biol. Chem.* **294**, 5813–5826 (2019).

73. N. O. Knudsen et al., Nuclear localization of human DNA mismatch repair protein exonuclease 1 (hEXO1). *Nucleic Acids Res.* **35**, 2609–2619 (2007).

74. N. O. Knudsen, S. D. Andersen, A. Lützen, F. C. Nielsen, L. J. Rasmussen, Nuclear translocation contributes to regulation of DNA excision repair activities. *DNA Repair (Amst.)* **8**, 682–689 (2009).

75. T. Li, B. A. Diner, J. Chen, I. M. Cristea, Acetylation modulates cellular distribution and DNA sensing ability of interferon-inducible protein IFI16. *Proc. Natl. Acad. Sci. U.S.A.* **109**, 10558–10563 (2012).

76. M. G. di Bari et al., c-Abl acetylation by histone acetyltransferases regulates its nuclear-cytoplasmic localization. *EMBO Rep.* **7**, 727–733 (2006).

77. M. Ishfaq et al., Acetylation regulates subcellular localization of eukaryotic translation initiation factor 5A (eIF5A). *FEBS Lett.* **586**, 3236–3241 (2012).

78. A. Pickard, P. P. Wong, D. J. McCance, Acetylation of Rb by PCAF is required for nuclear localization and keratinocyte differentiation. *J. Cell Sci.* **123**, 3718–3726 (2010).

79. A. M. Gacy, G. Goellner, N. Juranić, S. Macura, C. T. McMurray, Trinucleotide repeats that expand in human disease form hairpin structures in vitro. *Cell* **81**, 533–540 (1995).

80. J. T. Drummond, J. Genschel, E. Wolf, P. Modrich, DHFR/MSH3 amplification in methotrexate-resistant cells alters the hMutSalpha/hMutSbeta ratio and reduces the efficiency of base-base mismatch repair. *Proc. Natl. Acad. Sci. U.S.A.* **94**, 10144–10149 (1997).

81. J. Genschel, S. J. Littman, J. T. Drummond, P. Modrich, Isolation of MutSbeta from human cells and comparison of the mismatch repair specificities of MutSbeta and MutSalpha. *J. Biol. Chem.* **273**, 19895–19901 (1998).

82. G. B. Panigrahi, R. Lau, S. E. Montgomery, M. R. Leonard, C. E. Pearson, Slipped (CTG)*(CAG) repeats can be correctly repaired, escape repair or undergo error-prone repair. *Nat. Struct. Mol. Biol.* **12**, 654–662 (2005).

BIOCHEMISTRY

www.manaraa.com